CHAPTER VIII
NEW MOLECULAR THERMODYNAMIC MODEL FOR SOLUBILIZATION AND ADSOLUBILIZATION BY NOVEL IONIC SURFACTANT AGGREGATES*

8.1 Abstract

A new molecular thermodynamic model of micellar solubilization for simple hydrocarbon solutes was proposed. A treatment combined general solution thermodynamic principles with detailed molecular models for various contributions to free energy of aggregation (surfactant + solute), i.e. (1) surfactant-solute mixing (2) solute replacing water in the hydrated methylene layer of micelle (3) non-hydrated surfactant tail/aqueous interfacial tension reduction and (4) micellar core formation. Micelle was assumed as a pseudophase allowing a *priori* quantitative prediction for solubilization behavior of solutes by micelles starting from their molecular structures and the solution conditions. The solubilization locations of solutes and initial micellar properties were required as the main *priori* information. The solubilization was also assumed independent of micellar geometry change. This approach is more analytical while still providing acceptably accurately quantitative results. The validity of this model was verified by comparing model results with a number of experimental data. This approach accurately predicted solubilization isotherms without any fitting parameter, which no model has been done before. Moreover, this model was also valid for surface solubilization (or adsolubilization).

---

* Published in proceedings of APCChE 2006 conference

8.2 Introduction

Micellar solubilization refers to a phenomenon of an increase in the solubility of solvophobic solutes in an aqueous solution caused by a presence of micelles [1, 2]. The micelles provide a microenvironment conductive to the solute molecules, which are otherwise sparingly soluble in an aqueous solution. It is of important in many industrial, pharmaceutical and biological applications.

Since 1846 that the concept of micellar solubilization has been firstly traced, researchers have developed many methods to evaluate and/or predict the solubilization. Developments in the theory of solutions have led to the use of models involving solubility parameters to describe intramicellar solution.

Molar solubilization ratio was used to illustrate the solubilization capacity of particular micellar solution for specific solutes [3]. A group contribution model was developed for the prediction of the maximum solubilization capacity of solutes in micellar solution using the structural formula of the solute and its Henry's law constant [4]. In 1991, a successful molecular thermodynamic model for solubilization of hydrocarbons in ionic surfactant micelles at solute saturation was proposed [5]. The model allowed a *priori* quantitative prediction of the aggregation behaviours of surfactant and solute, starting from their molecular structures and the solution conditions. The solubilization of nonpolar gases was also predicted by a similar molecular thermodynamic approach [6]. A self-consistent mean field lattice theory of macromolecules was developed and modified for micellar solubilization to predict the maximum solubilization capacity [7]. This method is still qualitative and intensively computational. A lattice-based Monte Carlo method was used to qualitatively determine locus of solubilization [8]. Recently a net-average curvature model was proposed [9]. It was a combination of Kelvin equation of surface energy, the empirical surfactant affinity different equation and scaling law principles.

Most solubilization models to date are still qualitative and valid for the solubilization at solute saturation only. In reality, the partitioning nature of solutes varies by solute concentration in bulk aqueous and micellar phases. This work therefore aimed to develop a new approach to predict solute partitioning behaviours varied by solute concentration.

8.3 Thermodynamic Modeling

8.3.1 Ionic Micelle Model

The micelle of ionic surfactants is not a static but rather a constantly fluctuating system. The micelles contain sufficiently many surfactant molecules that the properties of the micelles approach those of a macroscopic system assumed as pseudophase. The micelle is characterized by four regions as shown in Figure 8.1 [10, 11].

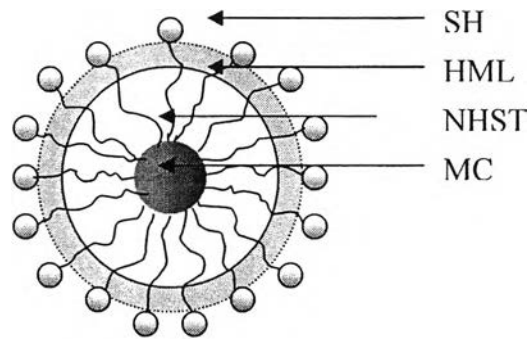

Figure 8.1 Typical ionic micelle model with four loci of solubilization.

The outer region is called surfactant head group (SH) region, which possesses the most polarity, consists of the surfactant head groups and counterions forming micelle-water interface including diffusive ionic cloud. It prefers highly polar solute partitioning. The inner region (micellar interior) is normally assumed as liquid-like. Only α-methylene groups of surfactant tails are hydrated [12]; creating an intermediate polar region called hydrated methylene layer (HML), which thus prefers an intermediate polar solute partitioning. The combined regions between hydrated methylene layer and surfactant head group regions is called "aqueous region". The deeper region among pure surfactant chains excluding α-methylene groups is dried and non-polar in nature called non-hydrated surfactant tail (NHST) region. It preferentially accommodates non-polar solute partitioning. However, micellar interior has a limited volume for solute. It becomes saturated and the pure solute droplet then exists at micelle centre called micellar core (MC) [13].

In summary, this solubilization model defined the solubilization location as consisting of four main regions; i.e., surfactant head (SH), hydrated methylene layer (HML), non-hydrated surfactant tail (NHST) and micellar core (MC) regions.

8.3.2 Thermodynamic Framework of Solubilization

The aggregation number of ionic micelles has been shown to change very little during solubilization although the aqueous solubility of hydrocarbon solute (without functional group), e.g. benzene, was reached [14]. Micelle geometric change was thus considered insignificantly. Consequently, thermodynamic analysis could be undergone by reasonable ignoring the effect of micelle geometric change due to solubilization. At constant volume, pressure and temperature, the standard chemical potentials of solute in aqueous phase and in micellar phase at equilibrium are equal to each other [15],

$$\mu_{am} = \mu_{aw} \tag{8.1}$$

where μ_{aj}^{o} is standard chemical potential of a solute in the j phase, w (water) or m (micelle) and a represents solute. The aqueous phase was assumed as pure water since the concentrations of surfactant and solute in aqueous solution are very low. Hence,

$$kT(\ln \gamma_{am} X_{am}) + \mu_{am}^{o} = kT(\ln \gamma_{aw} X_{aw}) + \mu_{aw}^{o} \tag{8.2}$$

where k is Bolzmann's constant, T is temperature (K) and γ_{aj} is activity coefficient of solute in the j phase, m or w. Rearrangement gave

$$\ln K_p = \ln(\gamma_{aw} / \gamma_{am}) - \Delta\mu_{w\to m}^{o} / kT \tag{8.3}$$

where $K_p = X_{am} / X_{aw}$ is a partition coefficient of solute. $\Delta\mu^o_{w\to m}$ is the standard chemical potential change of solubilization for transferring a solute molecule from aqueous phase to micellar phase. Standard chemical potential changes used through this article were defined as the Gibbs free energy change *per solute molecule*. Assumed a perfect ideal (infinitely diluted) solution of solute in bulk aqueous phase [16], one obtained

$$\ln K_p = -\ln \gamma_{am} - \Delta\mu^o_{pure\to m} / kT - \ln X^{sat}_{aw} \tag{8.4}$$

X^{sat}_{aw} is a saturated mole fraction of the solute in bulk aqueous phase. $\Delta\mu^o_{pure\to m}$ is the standard chemical potential change for transferring a solute molecule from pure solute phase to micellar phase. As μ of molecules at any location of micellar phase must be equal at thermodynamic equilibrium, $\Delta\mu^o_{pure\to m}$ is thus equal to the standard chemical potential change of solubilization for transferring a solute molecule from pure solute phase to NHST region, $\Delta\mu^o_{pure\to NHST}$, at equilibrium. The latter term was used through the rest of this article instead of the first term for the convenience in chemical potential determination. The NHST region consists of only non-hydrated surfactant alkyl chains and solute molecules. The value of $\ln\gamma_{am}$ for non-ideal binary mixture of solute and surfactant tails could be easily calculated by UNIFAC method [17].

The values of molecular parameters of all molecules were assumed indifferent between the molecules at non-equilibrium and equilibrium states, thus the minimization of chemical potential change to obtain equilibrium state was not needed to be performed. With known initial micellar properties and molecular parameters of solute and surfactant, this method minimized a number of our variables to only 1, i.e. intramicellar mole fraction of solute, X_{am}, at constant temperature. This approach allows us to reproduce the modified solubilization isotherms, $\ln K_p$-X_{am} curves, conveniently.

8.3.3 Standard Chemical Potential Change of Solubilization

Based on the proposed ionic micelle model, the $\Delta\mu^{o}_{pure\rightarrow NHST}$ ($=\Delta\mu^{o}_{pure\rightarrow m}$) was described in detail specifically for each solute, i.e. benzene, styrene and n-alkanes. The individual contributions of standard chemical potential change were based on known solubilization locations for each solute.

For benzene, experimentally, it was initially solubilized in surfactant tail region near micelle/water interface (assumed HML region) and then further solubilized toward NHST region upon increasing the intramicellar mole fraction of benzene or total benzene concentration [18]. These phenomena were also expected for other small aromatic molecules without functional group, e.g. styrene. Accordingly, a systematic thermodynamic pathway for transferring a solute molecule from its pure phase to micellar phase was proposed to determine $\Delta\mu^{o}_{pure\rightarrow NHST}$.

Step (1) benzene molecules transfer from pure benzene phase passing through the initial NHST/aqueous interface to NHST region. All benzene molecules mix with surfactant alkyl tails in micelles [positive effect to K_p].

Step (2) benzene molecules in NHST region move back toward HML region and thus insert their –CH group into HML region. This process involves a removal of those water molecules, which presumably are present initially in HML region. It is a withdrawal of benzene molecules from NHST region [negative effect to K_p]. This phenomenon still obeys the approximation in this step if

$$X_{CH\_HML} / X_{CH_2\_HML} = X_{am} / X_{STm} \tag{8.5}$$

where X_{STm} is a mole fraction of surfactant tail in micellar interior, X_{CH_HML} is a mole fraction of benzene –CH group in HML region and X_{CH2_HML} is a mole fraction of α-methylene group of surfactant tail in HML region.

Step (3) NHST/HML (aqueous region ~ water) interfacial tension reduces due to the presence of benzene at the interface releasing some benzene molecules from NHST region to aqueous region [negative effect to K_p].

Equivalent to this pathway, $\Delta\mu^{o}_{pure\rightarrow m}$ for benzene solubilization could be determined by combining those three contributions, i.e. (1) surfactant alkyl tail-benzene mixing $\Delta\mu^{o}_{mix}$ for step 1, (2) benzene -CH insertion in HML region $\Delta\mu^{o}_{HML}$ for step 2 and (3) NHST/aqueous interfacial tension reduction $\Delta\mu^{o}_{int}$ for step 3 as shown.

$$\Delta\mu^{o}_{pure\rightarrow m} = \Delta\mu^{o}_{mix} + \Delta\mu^{o}_{HML} + \Delta\mu^{o}_{int} \tag{8.6}$$

At high benzene concentration, MC region existed [14]. However, benzene molecules in MC region were believed that they all are still in contact with surfactant tails for benzene/surfactant ratio << 1 consistent with very small micellar core observed from Nagarajan's model for benzene solubilization at saturation [3].

In the case of n-alkanes, they were initially solubilized into MC region of ionic micelle [1, 10] and thus form NHST/MC interface. No n-alkane molecule exposes to water, $\Delta\mu^{o}_{HML}$ is thus zero. Very little amount of n-alkane in surfactant tail region was ignored. These processes are the removal of n-alkane molecules from NHST region. This case is different from the case of benzene because the solute distribution in micellar interior is non-uniform. The NHST/MC interface is also form and therefore new standard chemical potential change due to NHST/MC interface formation has to be defined as $\Delta\mu^{o}_{NHST/MC}$ (negative effect to K_p). The $\Delta\mu^{o}_{int}$ was neglected if no n-alkane molecule present in NHST and HML regions. $\Delta\mu^{o}_{mix}$ was differently defined as $\Delta\mu^{o}_{mix,MC}$ due to non-uniform distribution of n-alkane in micellar interior discussed later. Hence, $\Delta\mu^{o}_{pure\rightarrow m}$ for n-alkane solubilization is

$$\Delta\mu^{o}_{pure\rightarrow m} = \Delta\mu^{o}_{mix,MC} + \Delta\mu^{o}_{NHST/MC} \tag{8.7}$$

8.3.3.1 Surfactant Tail-Solute Mixing $\Delta\mu^{o}_{mix}$

The standard chemical potential change of solute-surfactant tail mixing in NHST region was divided into two correlations. The first one [19] is

$$\Delta\mu^{o}_{mix} / kT = [\ln\eta + (1-1/z)(1-\eta)] + [\chi_{as}(1-\eta)^2] \quad (8.8)$$

where z is a number of segments in a surfactant tail, as determined by $z = v_s / v_a$. v_s and v_a are molecular volume of surfactant tail and solute respectively. η is a volume fraction of solute in micelle. χ_{as} is an interaction parameter for solute and surfactant alkyl tail interaction. This correlation is valid for solubilization system which all solute molecules contact with surfactant tails and mix with surfactant tails homogeneously in surfactant tail region.

If solute distribution in micelles is not uniform; MC formation exists with lack, e.g. solubilization of n-alkanes, the chemical potential change cannot be directly calculated. It was known that the increment in the surface area of the micellar core brought about by the incorporation of an n-alkane solute molecule was constant for solubilization type II in ionic micelles [20]. The increment area was about the cross-sectional area of surfactant alkyl tail. This implies that the incorporation of one solute molecule produced the volume increment of surfactant tail region approximately equal to the volume of one surfactant tail. Thus, the chemical potential change of MC formation "per solute molecule" is approximately equal to that "per surfactant molecule" for uniform surfactant distribution in micelle. One obtains [5]

$$\Delta\mu^{o}_{mix,MC} / kT = [\ln(1-\eta) + X_{am}/(1-X_{am})\ln\eta] + [\chi_{as}(v_s / v_a)\eta] \quad (8.9)$$

(per surfactant molecule=per solute molecule)

8.3.3.2 Benzene -CH Insertion into HML Region $\Delta\mu^{o}_{HML}$

This contribution exists due to benzene molecules replacing water molecules in HML region upon increasing benzene mole fraction in micelles. Only one –CH group of benzene per solubilized benzene molecule was allowed to locate at HML region due to the limited thickness of HML. The approximation begins from the determination of water mole fraction in HML region. The mole fraction could be determined by Maxwell-Garnett and Bruggeman mixing rules with known equilibrium dielectric constant of HML region [21].

There are three components in HML region, which are benzene –CH group, surfactant α-methylene group and water molecules. To transform $\Delta\mu^{o}_{HML}$ to be a function of X_{am} instead of X_{CH_HML}, one assumed X_{CH_HML} $/X_{CH2\_HML} \cong X_{am}/X_{STm} = q$. This assumption was approximately valid even for deeper solubilization in NHST and MC regions if benzene molecules mix with surfactant tail homogeneously. This approximation will be proved by comparing with the experimental $\ln K_p$-X_{am} curves in results and discussion sections. By mole balance,

$$X_{CH\_HML} + X_{CH_2HML} + X_{w\_HML} = 1 \qquad (8.10)$$

where X_{w_HML} is mole fraction of water in HML region.

Thus,

$$X_{CH_2HML} = v_w /[v_{CH_2} / f - \frac{q v_{CH} v_{CH_2}}{v_w} + q v_w + v_w - v_{CH_2}] \qquad (8.11)$$

where f is a volume fraction of α-methylene group of surfactant tails in HML region, assumed constant since α-methylene group is a part of surfactant tail and micellar geometry does not significantly change upon solubilization. In this model, v_{CH_2}, v_w and v_{CH} are 26.9, 30.01 and 24.77 cubic angstrom at 298 K, respectively. Then,

$$X_{CH\_HML} = qX_{CH_2\_HML} \tag{8.12}$$

Considering those above equations, one can solve for all Xs in HML region if q is known. Finally, substituting X_{CH_HML} into (7.13) gives $\Delta\mu^{o}_{HML}$,

$$\Delta\mu^{o}_{HML} / kT = \Delta\mu^{o}_{CH\_HML} / kT = -\gamma_{CH\_HML} X_{CH\_HML} \tag{8.13}$$

where γ_{CH_HML} is activity coefficient of benzene –CH group in HML region calculated by UNIFAC method.

8.3.3.3 NHST/HML (Aqueous) Interfacial Tension Reduction $\Delta\mu^{o}_{int}$

This contribution was calculated as the product of solute cross-sectional area A_a in contact with the aqueous solution at equilibrium (assumed as a weak function of X_{am}) and the difference between the NHST/aqueous interfacial tension after solubilization σ_{as} and before solubilisation σ_{bs}.

$$\Delta\mu^{o}_{int} / kT = -A_a(\sigma_{as} - \sigma_{bs}) / kT \tag{8.14}$$

The value of σ_{as} could be estimated using a Prigogine theory applied by Nagarajan and Ruckenstien [5]. From this equation, σ_{as} decreases when X_{am} increases in surfactant tail region (~NHST) until some X_{am} that NHST region is saturated. Then X_{am} for NHST region is therefore presumably constant during MC formation resulting in constant $\Delta\mu^{o}_{int}$ after MC formation point, while $\Delta\mu^{o}_{HML}$ still keeps changing.

8.3.3.4 NHST/MC Interface Formation $\Delta\mu^{o}_{NHST/MC}$ [10]

This contribution is included for solute partitioning initially in MC region only, e.g. n-alkanes. $\Delta\mu^{o}_{NHST/MC}$ in this work was calculated from the

value of the macroscopic interfacial tension between water and pure solute molecules.

$$\Delta\mu^{o}_{NHST/MC} / kT = (\sigma_{aw} - 18)A_{a,\min} \tag{8.15}$$

$A_{a,\min}$ is a minimum interfacial area for the solute molecule, which was determined as a cross-sectional area of spherical van der Waals volume of the solute. The value 18 is a typical value of NHST/aqueous interfacial tension of *closest packed lamellae* consistent with dense packing nature of surfactant tails in micellar core.

8.3.4 Approximating Micellar Core Formation Point

Micellar core formation locally involves solute mixing with ending segments of surfactant chains in dried micellar interior only. This phenomenon is thus a competition between (1) miscibility between solutes and surfactant tail ends at the centre of micellar interior; promoting homogeneous mixing or inhibiting MC formation and (2) NHST-aqueous interfacial tension reduction promoting MC formation. Accordingly, it could be shown that at equilibrium of micellar core formation point,

$$\Delta\mu^{o}_{\text{int}} + \Delta\mu^{o}_{mix,ES} = 0 \tag{7.16}$$

where $\Delta\mu^{o}_{mix,ES}$ is a standard chemical potential change of the *end segment* of closely packed surfactant tails mixing with solute molecules. The end segment of surfactant tail, termed effective segment, was taken to consist of 3.6 methylene units [22]. The solubility parameter of end segment for calculating the enthalpy of mixing is approximately equal to that of C_3H_8 ($13.091*10^{-7}$ $(J/cm^3)^{0.5}$). This constraint will provide an initial point of micellar core formation. However, it is valid only for the cases of (1) solute molecules are initially solubilized at micellar interior near micelle-aqueous interface and occupying intramicellar space homogeneously, e.g. benzene

solubilized in ionic micelles and (2) very small water mole fraction in micelles; only α-methylene groups of surfactant tails are hydrated due to closely packing of surfactant molecules, e.g. C_{16+}TAB.

8.4 Model Validation and Discussion

In this section, the proposed molecular thermodynamic theory of solubilization was validated by implementing it in cases of well-understood hydrocarbon solutes in ionic surfactant aqueous solutions listed in Table 8.1. All molecular parameters and physical properties were shown in Table 8.2 and 8.3. The primary objective now is to assess the proposed model with the experimental modified solubilization isotherms, $\ln K_p$-X_{am} correlation.

Table 8.1 Experimental solubilization data.

Solute	Surfactant	Temperature (°C)	References
Benzene	CTAB	25	[24]
Benzene	CPC	25	[24]
Benzene	SDS	25	[24]
n-Hexane	CPC	25	[1]

Table 8.2 Physicochemical properties of solutes at 25 °C [23]

	Benzene	Styrene	n-Pentane	n-Hexane	n-Heptane
Molecular volume (A^3)	148.65 (liq)[a]	192.22 (liq)[a]	96.40 (vdW)[b]	113.39 (vdW)[b]	130.38 (vdW)[b]
Molecular weight (g/g mol)	78.1134	104.152	72.15	86.177	100.204
Solubility parameter ($(J/cm^3)^{0.5}$)	18.706	19.127	14.439	14.988	15.208
Solubility in water (mol fraction)	4.16×10^{-4}	4.52×10^{-5} (30°C)[c]	9.61×10^{-6}	1.98×10^{-6}	4.03×10^{-7}
Cross sectional area A (A^2/molecule)	28.35 (vdW)	40.27 (liq)	25.42 (vdW)	28.32 (vdW)	31.09 (vdW)
Surface tension (dyne/cm)	28.21	31.54 (30°)	15.47	17.98	19.78

[a] (liq) = calculated from assumed-spherical liquid volume or area per molecule

[b] (vdW) = calculated from assumed-spherical van der Waals volume or area per molecule

[c] extrapolated from the solubility of styrene ranging from 160 mg/L at 23°C to 310 mg/L at 20°C

Table 8.3 Physicochemical properties of water and surfactant tails at 25 °C.

	Water	Surfactant tail in NHST region	
		$n\text{-}C_{15}$	$n\text{-}C_{11}$
Molecular volume (A^3)	30.01	431.2	352.3
Molecular weight (g/g mol)	18.0152	211.4	156.3
Solubility parameter $((J/cm^3)^{0.5})$	47.813	15.9[a]	16.0[a]
Surface tension (dyne/cm)	73.56	28.2082[a]	24.24[a]

[a] assumed equivalent to the properties of n-alkane with the same carbon number

Table 8.4 Experimental adsolubilization data.

Solute	Surfactant	Temperature (°C)	Solid Substrate	References
Styrene	CTAB	30	Silica	[25]
n-Pentane	SDS	25	Alumina	[26]
n-Pentane	SDS	25	Alumina	[26]
n-Heptane	SDS	25	Alumina	[26]

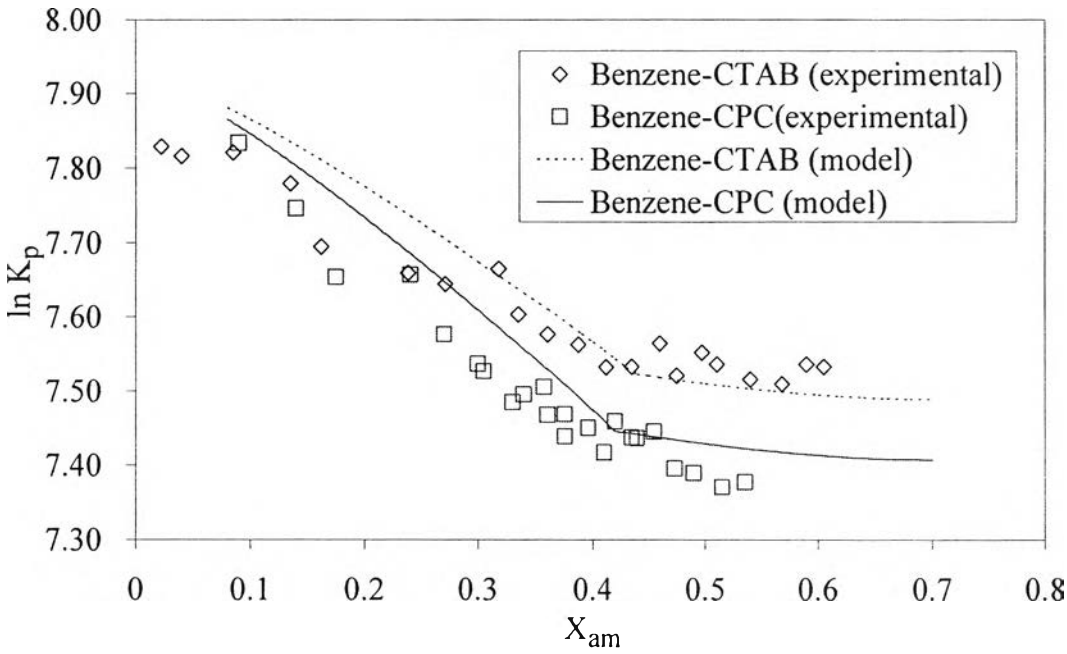

Figure 8.2 Solubilization of benzene in CTAB and CPC micelles.

For benzene s olubilization in cetyltrimethylammonium bromide (CTAB) and cetylpyridinium chloride (CPC) micelles shown in Figure 8.2, benzene partition coefficient K_p decreased upon increasing benzene mole fraction in CTAB micelles X_{am}. This is consistent with theory stating that the presence of benzene in the NHST region inhibits subsequent solubilization. As more benzene was added, the benzene molecules tended to be solubilized deeper in the surfactant tail region. The surfactant tail region then became saturated and a droplet of benzene then formed MC region within the micelle. The MC formation occurred such that curve of lnK_P showed an inflection change when X_{am} is ~ 0.4 which was consistent with NMR spectroscopy ($0.4<X_{am}<0.55$) [18].

Based on the experimental information, benzene molecules in this model partition into surfactant tail region only. The initial interfacial tension at the NHST/aqueous region interface σ_{bs} was calculated by using correlation $\sigma_{bs} = \sigma_s + \sigma_w - 2\psi(\sigma_s\sigma_w)^{1/2}$ where σ_s is a surface tension of the NHST and assumed equal to that of n-alkane with the same carbon number; that is, 51.51 mN/m for CTAB micelle. The dielectric constant of the HML region was assumed equal to

that of closely pack hydrated CTAB monolayer adsorbed on mica surface; 0.36 [27]. By Maxwell-Garnett and Bruggeman mixing rules, the water mole fraction in HML was calculated as 0.6. The molecular volumes of benzene incorporating in $\Delta\mu^{o}_{mix}$ and $\Delta\mu^{o}_{int}$ were assumed as liquid volume. However, the cross-sectional area per benzene molecule at NHST/aqueous interface was calculated from van der Waals volume because of strong negative charge density (π-electron) of benzene ring strongly attracting cationic surfactant head, thus producing very dense micellar packing [18]. It was observed that the calculated $\ln K_P$ always decreased with increasing X_{am}, which fit very well with the experimental results. According to this model, the retardation of solubilization was governed by dominant effects of decreasing ($-\Delta\mu^{o}_{int}$) and ($-\Delta\mu^{o}_{mix}$) over ($-\Delta\mu^{o}_{HML}$), whereas the change in an activity coefficient of benzene in NHST region was rather small compared with the other contributions and might be ignored. The model provided MC formation point at X_{am}= 0.44, which is close to the experimental result from $\ln K_p$-X_{am} curve (X_{am}=0.43) and NMR spectroscopy ($0.4<X_{am}<0.55$). This implies that CTAB head groups do not have a significant effect on MC formation. After MC formation point, an effect of NHST/aqueous interfacial tension reduction was cancelled due to assuming a small effect of micellar curvature change after solute saturation in NHST region. All solubilized benzene molecules were still in contact with surfactant alkyl tail if solute/surfactant mole ratio in a micelle is much less than unity. This phenomenon after MC formation was driven by the $\Delta\mu^{o}_{HML}$ change (more benzene partitions into HML region, while no significant change occurs in NHST region). The fitting between the experimental and model results after MC formation point was very good supporting the effect of $\Delta\mu^{o}_{HML}$ and the assumption $X_{CH\_HML}/X_{CH2\_HML} \cong X_{am}/X_{STm}$ mentioned earlier.

Benzene solubilization in CPC micelle was similar to the results observed for CTAB micelle. The water mole fraction in HML region was assumed to be the same due to similarities in tail length and aggregation number. All molecular properties were also similar except σ_{bs}. The higher slope of $\ln K_p$ vs X_{am} curve is due to the higher σ_{bs}, 55 mN/m for cylindrical CPC micelle [12]. The predicted MC

formation point was at X_{am} = 0.41 which is lower than that of benzene in CTAB micelles. This means the NHST/aqueous interface in the CPC micelle can be more easily expanded toward the bulk aqueous phase. After the MC formation point the model results continue fitting well.

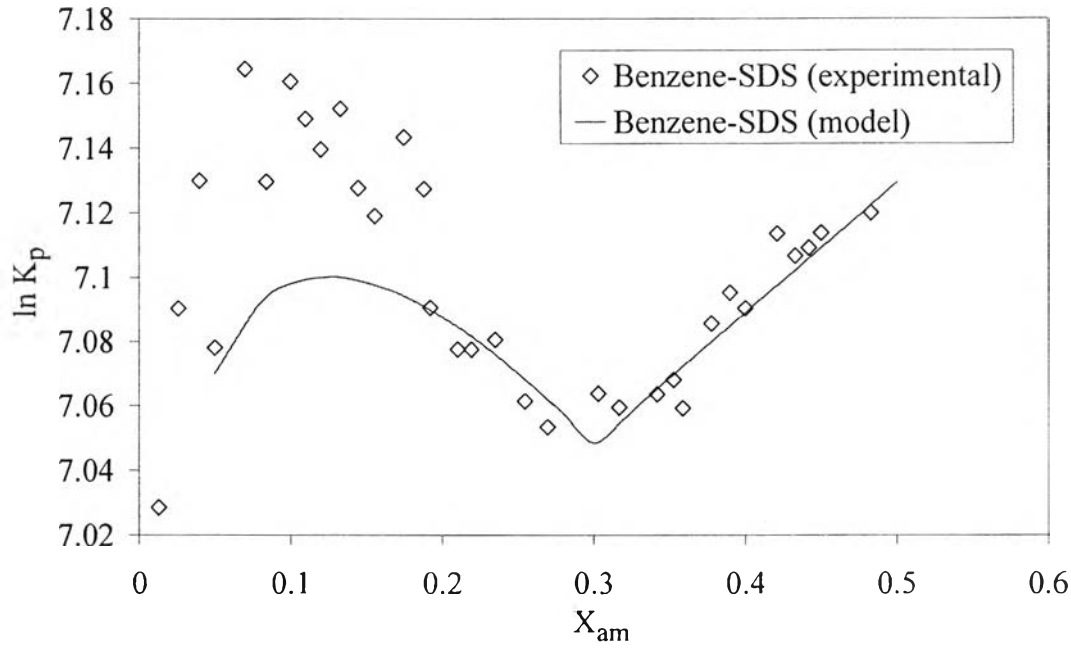

Figure 8.3 Solubilization of benzene in SDS micelles.

Benzene solubilization behavior in sodiumdodecyl sulphate (SDS) micelles was significantly different from that observed in CTAB and CPC micellar systems (Figure 8.3) because the significant hydration of the polar heads produces a rather ill-defined NHST/aqueous interface [11]. This reflects in the high water mole fraction in the HML region demonstrating in its higher dielectric constant (~65% higher than that of CTAB and CPC micelles). However, it was still assumed that only α-methylene groups in surfactant tails were hydrated and benzene molecules were initially solubilized in the micelle interior close to NHST/aqueous interface. Figure 8.3 shows that at very low benzene concentrations, $\ln K_p$ increased upon increasing X_{am}. The major effect at small X_{am} mainly came from $\Delta\mu^{o}_{HML}$ because benzene was initially solubilized at NHST/aqueous interface. At intermediate benzene

concentrations, $\ln K_p$ decreased with increasing X_{am} as benzene was solubilized deeper into NHST region. This process was controlled by benzene-surfactant tail mixing, $\Delta\mu^{o}_{mix}$. The MC formation point was calculated as ~0.6 which was different from experimental data, ~0.3. The possible reason behind this error is the deep penetration of water into surfactant tail region within SDS micelles. The micellar interior thus provides lower stability than expected because of incompatibility between water and surfactant alkyl tail in micelles. We could not predict MC formation point due to lack information of the water penetration. However, the experimental value, X_{am}=0.3 was applied to the model instead. After MC formation point, $\ln K_p$ increased monotonically and fit very well with the experimental results supporting the assumption of $\Delta\mu^{o}_{HML}$ even though the micelles contain large amount of water molecules.

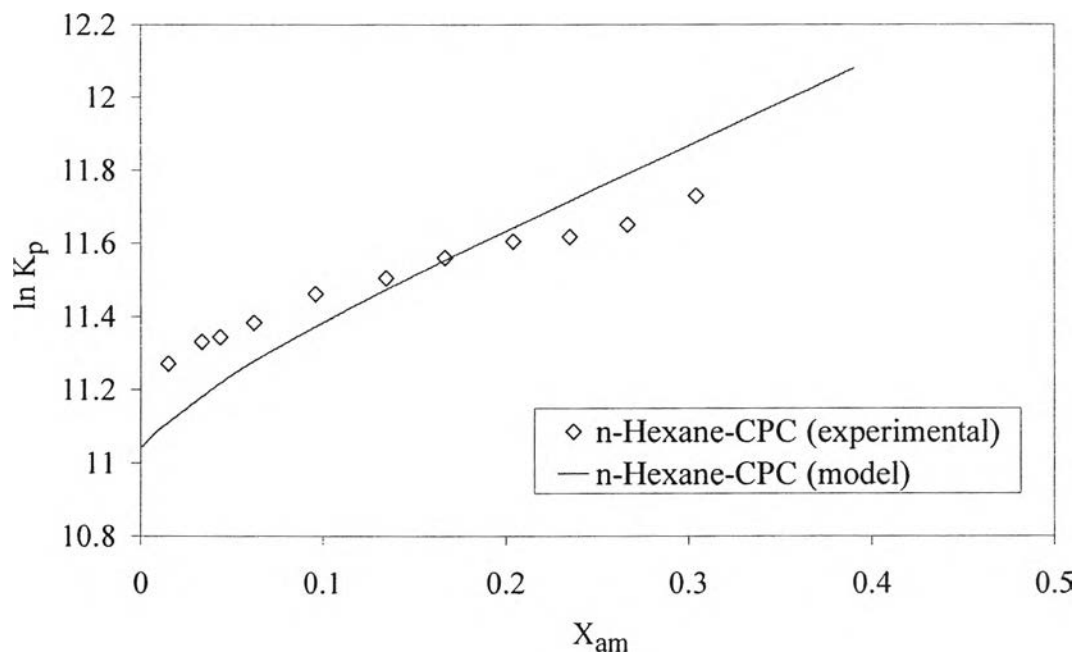

Figure 8.4 Solubilization of n-hexane in CPC micelles.

For n-hexane solubilization in CPC micelles shown in Figure 8.4, $\ln K_p$ increased upon increasing X_{am} leading to a conclusion that n-hexane was solubilized

at the MC region of CPC micelles. Based on this known solubilization location, it was assumed that there was no n-hexane molecule in HML region and at NHST/aqueous interface. $\Delta\mu^{o}_{HML}$ and $\Delta\mu^{o}_{int}$ consequently were reasonably ignored. The $\Delta\mu^{o}_{mix,MC}$ was used instead of $\Delta\mu^{o}_{mix}$. It was found that $\ln K_p$-X_{am} fitted very well with experimental result. The increase in $\ln K_p$ was controlled by $\Delta\mu^{o}_{mix,MC}$ increasing in magnitude.

Additionally, this model was also applied to the similar solubilization phenomenon at solid surface called "adsolubilization" by assuming similar properties between micelle and admicelle (see The similar typical structure of an admicelle with its loci of adsolubilization in Figure 8.5) it. The reference systems were listed in Table 8.4. The model still showed good agreement with these adsolubilization systems as shown in Figure 8.6 and 8.7.

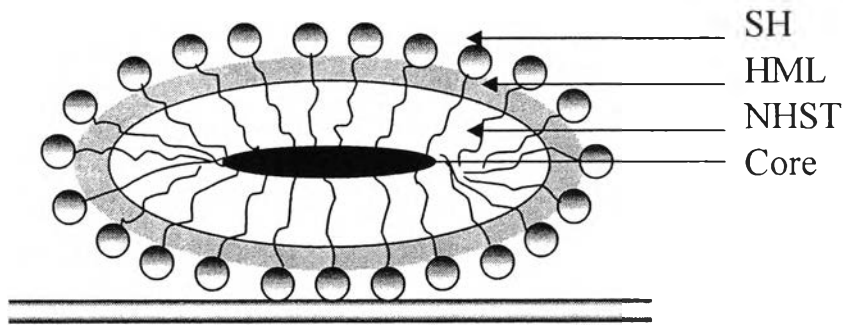

Figure 8.5 Typical ionic admicelle model with four loci of adsolubilization.

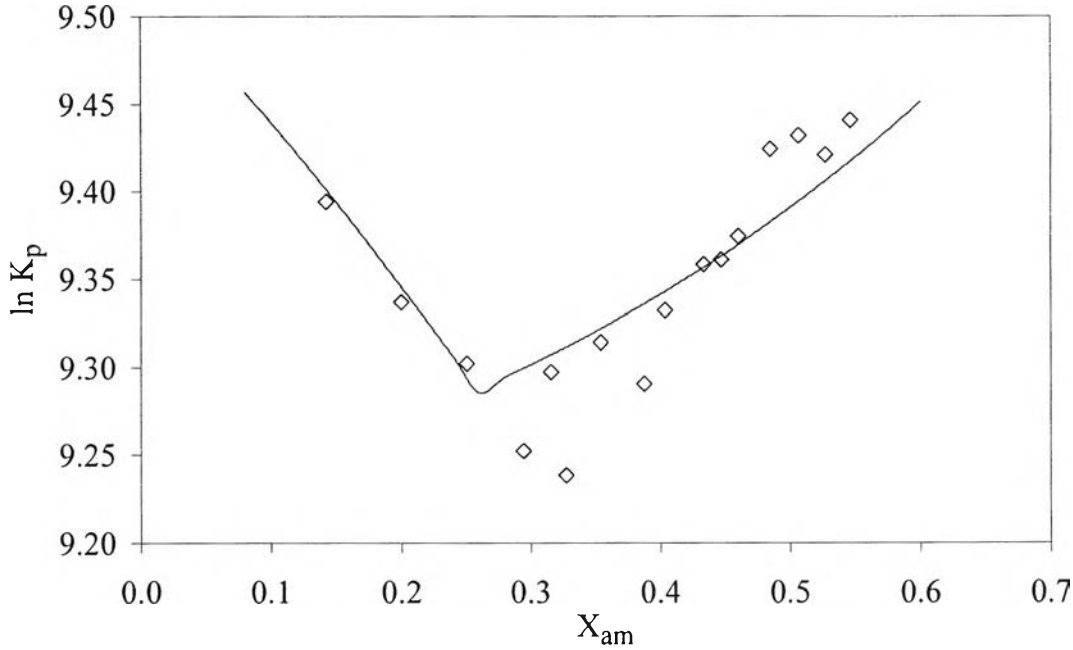

Figure 8.6 Adsolubilization of styrene in CTAB admicelles.

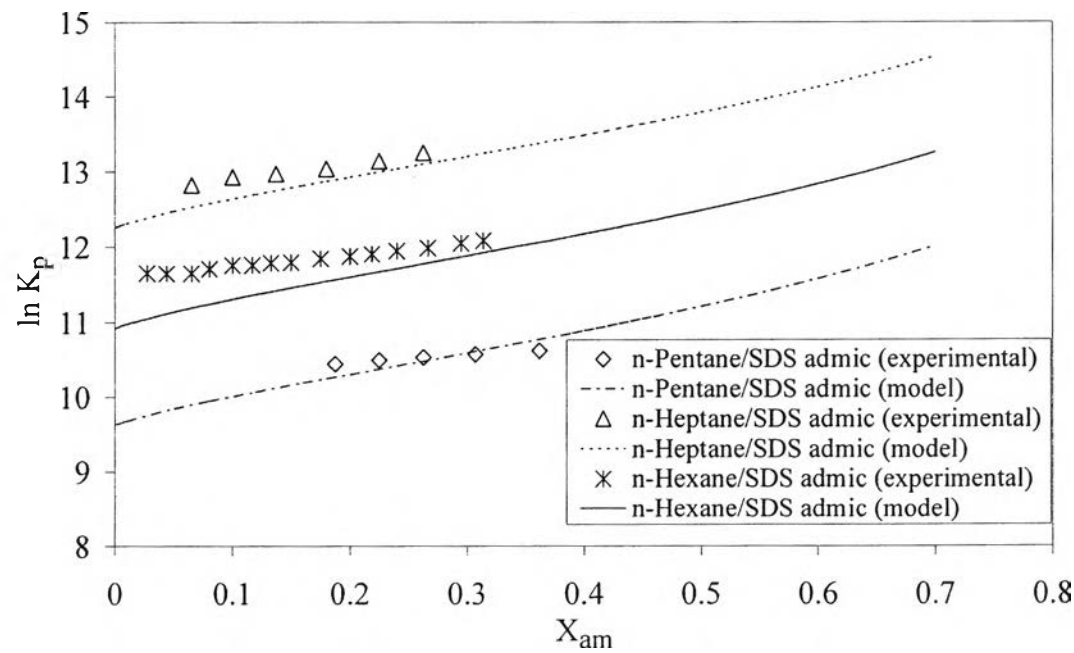

Figure 8.7 Adsolubilization of n-alkanes in SDS admicelles.

8.5 Conclusions

The chemical potential change of solubilization consists of (1) surfactant-solute mixing (2) solute replacing water in the hydrated methylene layer of micelle (3) non-hydrated surfactant tail/aqueous interfacial tension reduction and (4) micellar core formation. Micelle was assumed as pseudophase. The solubilization locations for solutes, initial micellar properties and molecular properties were required as the initial inputs. The solubilization was also assumed independent of micellar geometry change. Applying the chemical potential changes to the equilibrium equation provided accurate $\ln K_p$-*Xam* isotherms without any fitting parameter. However, this model is valid for aqueous system containing *densely packed* surfactant aggregates and *simple* solute only.

8.6 Acknowledgment

We are grateful to the Thailand Research Fund (TRF) for financial support through the Royal Golden Jubilee Ph.D. Program (Grant No. PHD/0217/2544).

8.7 References

[1] S.D. Christian, J.F. Scamehorn, Solubilization in Surfactant Aggregates, Marcel Deckker, New York, 1995.

[2] M.J. Rosen, Surfactants and interfacial phenomena, second ed., John Wiley & Sons, New York, 1989.

[3] R. Nagarajan, M.A. Chaiko, E. Ruckenstein, J. Phys. Chem. 88 (1984) 2916-2922.

[4] G.A. Smith, S.D. Christian, E.E. Tucker, Langmuir 3 (1987) 598-599.

[5] R. Nagarajan, E. Ruckenstien, Langmuir 7 (1991) 2934-2969.

[6] S. Roy, A. Mehra, D. Bhowmick, J. Colloid Interf. Sci. 196 (1997) 53-61.

[7] P.N. Hurter, T.A. Hatton, Langmuir 8 (1992) 1291-1299.

[8] S.K. Talsania, L.A. Rodríguez-Guadarrama, K.K. Mohanty, R. Rajagopalan, Langmuir 14 (1998) 2684-2692.

[9] E. Acosta, E. Szekeres, D.A. Sabatini, J.H. Hawell, Langmuir 19 (2003) 186-195.

[10] M. Aamodt, M. Landgren, B. Jonsson, J. Phys. Chem. 96 (1992) 945-950.

[11] H. Goncalves, A. Lattes, J. Phys. Chem. 95 (1991) 4557-4563.

[12] A. Heindl, H.H. Kohler, Langmuir 12 (1996) 2464-2477.

[13] Y. Doi, Y. Kawashima, K. Matsuoka, Y. Moroi, J. Phys. Chem. B 108 (2004) 2594-2599.

[14] K. Kandori, R.J. McCreevy, R.S. Schechter, J. Phys. Chem. 93 (1989) 1506-1510.

[15] G.G. Liu, D. Roy, M.J. Rosen, Langmuir 16 (2000) 3595-3605.

[16] R.A. Alberty, R.J. Silbey, Physical Chemistry, first ed., John Wiley & Sons, Singapore, 1992.

[17] J.M. Smith, H.C. Van Ness, M.M. Abbott, Introduction to Chemical Engineering Thermodynamics, fifth ed., McGraw-Hill, New York, 1996.

[18] N. Hedin, R. Sitnikov, I. Furo, U. Henriksson, O. Regev, J. Phys. Chem. B, 103 (1999) 9631-9639.

[19] V.J. Klenin, Thermodynamics of Systems Containing Flexible-Chain Polymers, first ed., Elsevier Science, New York, 199.

[20] N. Nishikidom, J. Colloid Interf. Sci., 131 (1989) 440-447.

[21] K. Kärkkäinen, A. Sihvola, K. Nikoskinen, K., IEEE Transactions on Geoscience and Remote Sensing, 39 (2001) 1013-1018.

[22] R.A. Johnson, R. Nagarajan, Colloid Surf. A 167 (2000) 31-46.

[23] C.L. Yaws, Chemical Properties Handbook, McGraw-Hill, New York, 1999.

[24] F. Gadelle, W.J. Koros, R.S. Schechter, J. Colloid Interf. Sci., 170 (1995) 57-64.

[25] B. Kittiyanan, J.H. O'Haver, J.H. Harwell, S. Osuwan, Langmuir, 12 (1996) 2162-2168.

[26] R. Sharma, Surfactant Adsorption and Surface Solubilization, ACS, Washington, DC. 1995.

[27] O. Teschke, G. Ceotto, E.F. de Souza, Chem. Phys. Lett. 344 (2001) 429-433.